

# Strain shielding and confined plasticity in thin polymer films: Impacts on thermomechanical data storage

S. Sills<sup>a</sup>, R.M. Overney<sup>a,\*</sup>, B. Gotsmann<sup>b</sup> and J. Frommer<sup>c</sup>

<sup>a</sup>Chemical Engineering, University of Washington, Box 351750, Seattle, WA 98195, USA

<sup>b</sup>IBM Research, Zurich Research Laboratories, Säumerstrasse 4, CH-8803 Rüschlikon, Switzerland

<sup>c</sup>IBM Research, Almaden Research Center, 650 Harry Rd, San Jose, CA 95120, USA

Received 15 April 2004; accepted 13 June 2004

Substrate constraints and interfacial boundary layers in thin polystyrene films are explored with high strain rate indentations characteristic of thermomechanical terabit data storage operations. Under these impact-like conditions, the coupling of strain-rate and inertial effects leads to large plastic deformations relative to quasi-static indentations. Strain shielding is present when the plastic deformation radius exceeds ~65% of the film thickness. Thereafter, deformation is restricted by the rigid substrate, giving rise to elevated rim heights and interfacial shearing. The shielding effects were alleviated with use of a modulus-matched buffer layer between the polymer film and the substrate. A non-monotonic rheological gradient in the polymer films leads to the distribution of contact pressures between two asymptotic scenarios: (i) a compliant surface with a rigid sub-surface and (ii) a rigid surface with a compliant sub-surface.

**KEY WORDS:** thermomechanical data storage, polymer thin films, interfacial confinement, substrate constraints, strain shielding, Scanning Probe Microscopy (SPM), indentation, pile-up

## 1. Introduction

Ultrahigh density thermomechanical data storage (TDS) is a novel recording scheme intended to circumvent the superparamagnetic limit associated with magnetic storage [1,2]. TDS relies on writing, reading, and erasing nanometer sized data bits in thin polymer films. In essence, TDS recording is a high speed (MHz), elastic–viscoplastic indentation process. The polymer storage media must be designed to achieve the narrow range of physiochemical properties necessary for: high data density, fast data rates, high durability, long shelf life, and low power consumption. The ideal polymer should be easily deformable for bit writing; however, the written bits must be stable against thermal degradation and wear.

Each indented bit represents a metastable state of the deformed volume, and will either initiate spontaneous dewetting (film instability) or strive for recovery of the initial unstressed state (bit instability) [3]. The delicate balance between these instability nodes constitutes one optimization scenario in the design of polymeric storage media. Furthermore, media (and data) wear must be minimized during scanning operations. In particular, topographical protrusions, in the form of piled-up *rims* around the indented bits, are regions susceptible to wear.

The presence of rims also adversely affects the writing density. Rims interact non-linearly with adjacent bits, lowering the signal-to-noise ratio of bit detection and requiring a relaxation of the indentation pitch (data density). From the perspectives of media wear and data density, a suitable polymer storage medium exhibits a weak propensity for rim formation during indentation.

In this letter, we explore how the contact mechanics associated with TDS in polymer films are compounded by the proximity of the underlying substrate. A rigid boundary interacting with the stress field during indentation (bit writing) may alter the imposed stress and strain distributions, leading to bulk-deviating mechanical responses [4–7]. For indentations in compliant films, increased rim heights are observed when elastic strain and plastic flow are constrained, or shielded, by a rigid substrate [4–7]. In the case of rigid films on compliant substrates, plastic yield of the underlying substrate accommodates an enhanced *sink-in* of the surface around the periphery of indentation sites [5]. Specifically, we investigate interfacial strain shielding and its implications on rim formation during high strain rate indentations in thin polystyrene films. We revisit the scaling basis of the “10% rule” for ascertaining substrate constraints under impact conditions. Finally, we illustrate the role of rheological anisotropy in the indentation process, and elucidate the polymers’ mechanical response with interfacial glass transition profiles.

\*To whom correspondence should be addressed.  
E-mail: roverney@u.washington.edu

## 2. Experimental

Polystyrene films (PS) ( $M_w = 12k$ ), 16–163 nm thick, were spin cast from cyclohexanone solutions onto silicon wafers ( $<100>$ , N-doped,  $0.1 \Omega/\text{cm}$ ). One sample (45 nm PS) was cast onto a 230 nm film of crosslinked polystyrene-vinylbenzocyclobutene (PS-BCB) to mask the silicon substrate in order to decouple substrate from film thickness affects. All films were annealed between 160 and 175 °C under argon for 30 min. The thin films were indented with a cantilevered probe setup identical to the ones used for TDS, figure 1.

The indenting probe was operated with a modified commercial scanning probe microscope (SPM) (DI Dimension 5000, Veeco). For this study, the indentations were created at room temperature. The normal indentation load,  $F_N$ , was provided through an electrostatic force generated with a bias between the substrate and the electrostatic plate on the lever. The magnitude of  $F_N$  is proportional to the square of the lever-sample bias,  $\Delta V$ , i.e.  $F_N(\Delta V) = \alpha|\Delta V|^2$ , where  $\alpha$  is a calibration constant. The lever is calibrated through a series of force–displacement (FD) curves conducted over a range of biases. For each FD curve, the electrostatic force is  $F_N(\Delta V) = C_N * \Delta z(\Delta V)$ , where  $C_N$  is the normal spring constant of the lever ( $\sim 0.1 \text{ N/m}$ ) and  $\Delta z(\Delta V)$  is the additional  $z$ -displacement required to reach the snap-out instability for a given bias, pictured in the inset of figure 2.

The indentation loads were provided in the form of 10  $\mu\text{s}$  pulses. A short pulse-time was chosen in accordance with operating rates used for TDS writing [2]. For each film thickness, arrays of  $10 \times 10$  indentations were generated at loads ranging from 50 to 250 nN. The uncertainty associated with the absolute force values is approximately  $\pm 20\%$ , but the relative uncertainty between force measurements is within 9%.

Topography images of the residual indentations were acquired using the same probe with the optical detection scheme of the SPM. Figure 3 illustrates such an indentation array for a 45 nm PS film on a 230 nm PS-BCB buffer film.

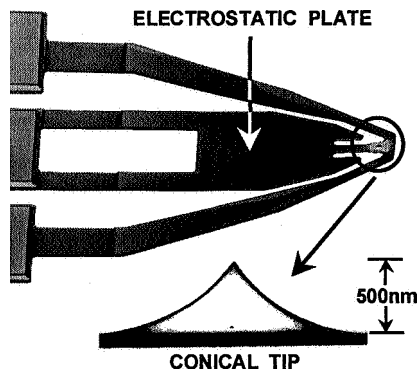


Figure 1. Scanning electron microscopy (SEM) images of the cantilever used in this study, a typical design for ultrahigh density thermomechanical recording. Loading is controlled via the bias between the electrostatic field plate and the sample substrate.

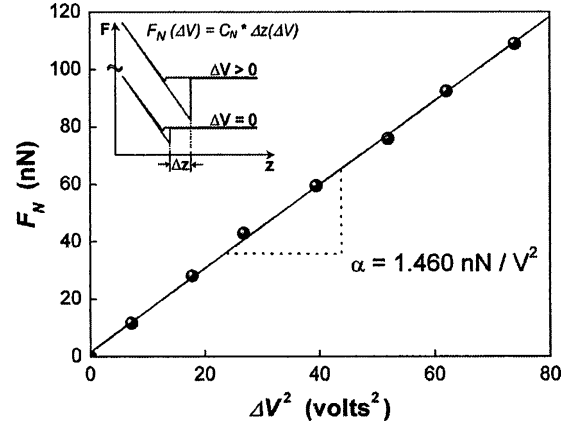


Figure 2. Electrostatic force calibration of the cantilever probe. (inset) The electrostatic force,  $F_N$  for a given bias,  $\Delta V$ , is determined from the additional displacement,  $\Delta z$ , necessary to reach the snap-out instability during a force–displacement curve ( $C_N$ =normal spring constant,  $\alpha$ =calibration constant).

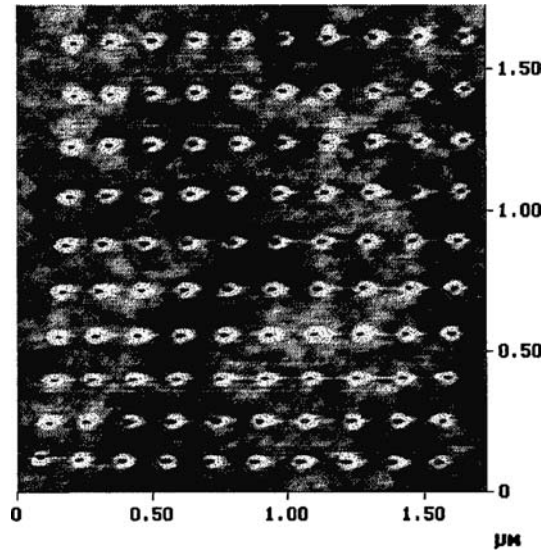


Figure 3. SFM image of a  $10 \times 10$  indentation array in a 45 nm PS film on a 230 nm crosslinked PS-BCB substrate (grayscale range = 15 nm).

Figure 4 illustrates the parameters deduced from each indentation, which are categorized into vertical parameters (indent depth,  $d$ , rim height,  $z$ ) and horizontal parameters (indent diameter,  $D_i$ , rim diameter,  $D_R$ ). The slight elliptical shape of the indentations, apparent in figure 4, results from the  $4^\circ$  relative cantilever-sample declination necessary to avoid optical interference on the photodiode. Because of this asymmetry, the geometric features for each indentation were measured at the four cardinal points and averaged. Individual datum points in subsequent figures represent a collective average of 20 indentations.

## 3. Results and discussion

The indentation parameters in a silicon-supported 69 nm film are correlated to the applied load in

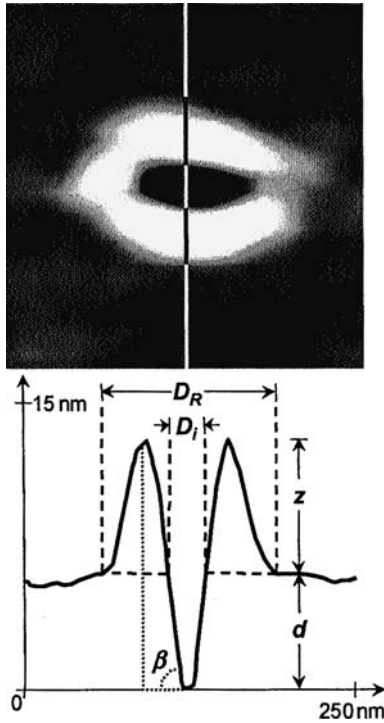


Figure 4. Geometric evaluation of residual indentations (45 nm PS on 230 nm of crosslinked PS BCB). Vertical parameters: rim height,  $z$ , and the indentation depth,  $d$ . Lateral parameters: rim diameter,  $D_R$ , and the indentation diameter,  $D_i$ .

figure 5, which is qualitatively representative of each film thickness and substrate configuration. Considering all sample thicknesses and indentation loads, the residual indentation depth ranged from 0.4 to 3.5 nm, with the rim height always some fraction of the depth. The residual indent diameter ranged from 15 to 50 nm, assuming negligible dilation by the imaging tip; while the rim diameter ranged from 70 to 160 nm. With an indenter aspect ratio close to one, the discrepancy in the magnitude between the vertical and lateral parameters suggests significant elastic recovery in the surface-normal

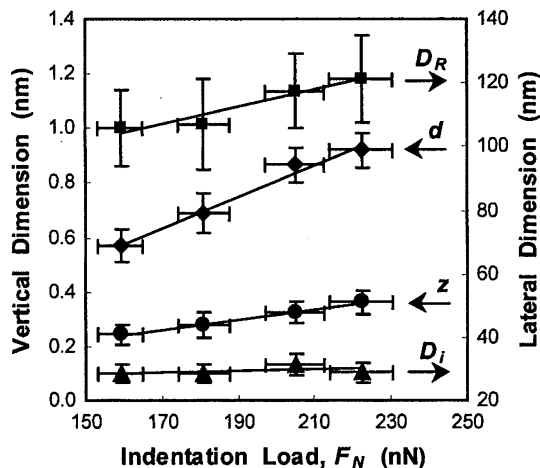


Figure 5. Load dependence of the vertical and lateral parameters of residual indentations in a silicon-supported, 69 nm PS film.

direction on unloading. However, in the discussion below, we will argue that it is the coupling of high strain-rates and inertia, not elastic recovery, that is responsible for the dimensional mismatch.

The extent of elastic versus plastic deformation can be estimated by considering the ratio of the strain imposed by the indenter to the strain capacity of the material [8]; i.e.  $E \tan \beta_{\text{TIP}}/Y$ , where  $E$  is the sample modulus,  $\beta_{\text{TIP}}$  is the excluded tip-sample angle (imposed strain), and  $Y$  is the material yield stress. Bulk PS under quasi-static conditions exhibits a 3.0 GPa [9] and 110 MPa [10] modulus and yield stress, respectively.  $\beta_{\text{TIP}}$  was determined with scanning electron microscopy to be  $52^\circ$ . Thus, assuming bulk material behavior, the imposed strain versus strain capacity ratio for this system is 38, which exceeds the critical value ( $\sim 30$ ) for fully plastic deformation [8]. Moreover, for a ratio of 38, the elastic-plastic indentation simulations of Ramond-Ang el elis indicate a uniform elastic recovery of roughly 10% in both the indent depth and diameter [11]. In addition, at high strain rates used in these experiments, the effect of strain rate hardening [12–14] is to increase the modulus over its quasi-static value, further reducing elastic recovery. Consequently, this suggests that elastic recovery is not responsible for the high radial aspect of the indentations.

The model above assumes a quasi-static indentation process, which does not apply to the fast indentation rates employed here. Assuming that the plastically deformed volume is hemispherical with a diameter,  $D_p$ , equal to the rim diameter,  $D_R$ , [7,8] we would expect the plastic zone diameter to range from 20 to 40 nm for quasi-static conditions. This is based on Johnson's cavity model for elastic-plastic indentation [8] pictured in figure 6 and on Nayebi's quasi-static plastic zone analysis, which relates  $D_p$  to the applied load and the material yield stress, through  $D_p = 2(F_N/(2\pi Y))^{1/2}$  [15].

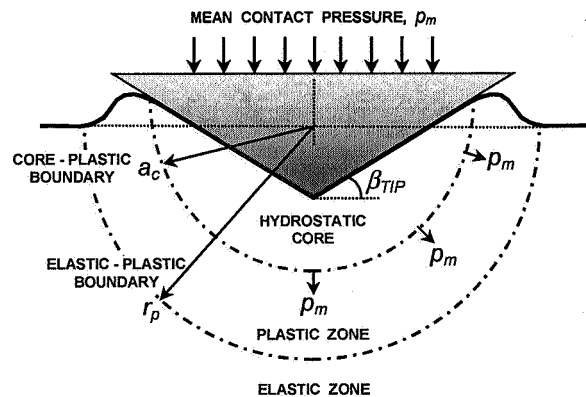


Figure 6. Cavity model of elastic-plastic indentation by a rigid cone. Directly beneath the contact, the pressure is supported by a hydrostatic core. Beyond the core, lies the plastic deformation zone, where the pressure exceeds the material yield stress by roughly three-fold [8]. The plastic front is preceded by elastic strain that accommodates pressures insufficient of producing yield,  $p_m$  is the mean contact pressure,  $a_c$  is the contact radius, and  $r_p$  is the plastic radius (1/2 the plastic diameter,  $D_p$ ).

The quasi-static case clearly underestimates the observed 70–60 nm rim diameter, and suggests that strain rate and inertial effects must be considered. Inertial effects are propagated through the material as stress waves; while strain-rate effects are attributed to a transition from thermally activated mechanisms to linear viscous mechanisms [16]. The strain rates ranged from  $2 \times 10^3$  to  $1 \times 10^4 \text{ s}^{-1}$ , determined from the residual strains (see below) and the  $10 \mu\text{s}$  indentation time. They exceed those of quasi-static indentation, and fall within the regime of impact dynamics [17]. The main difficulty with impact studies is that the inertial and strain-rate effects are usually coupled [18]. The characteristics of wave propagation inevitably depend on the strain-rate dependence of the material properties. At strain rates of  $10^3\text{--}10^4 \text{ s}^{-1}$ , polystyrene succumbs to viscoplastic flow at a nearly constant flow stress of  $\sim 20 \text{ MPa}$  [19]. This suggests that the propagation speed of a plastic stress wave,  $c_p(\sigma) = (1/\rho_o \partial\sigma/\partial\varepsilon)^{1/2}$  [17], approaches zero above the flow stress.  $\rho_o$  is the density of the unloaded material, and  $\partial\sigma/\partial\varepsilon$  is the slope of the stress–strain curve at a given strain and strain rate. Thus, any plastic stress waves generated in our study are likely to rapidly attenuate [17] (exponentially [20]) as they propagate from the impact site, while the energy carried by the pressure pulse is dissipated through plastic deformation processes [20].

Another important aspect is the role of the substrate during impact of thin films. Examining the ratio of the rim height to the indentation depth,  $z/d$ , provides an initial assessment of substrate constraints imposed during the indentation process. In figure 7, the  $z/d$  ratio is reported as a function of film thickness. The inset of figure 7 shows the ratio of the  $z(F_N)$  and  $d(F_N)$  slopes, which are determined from the linear fits represented in

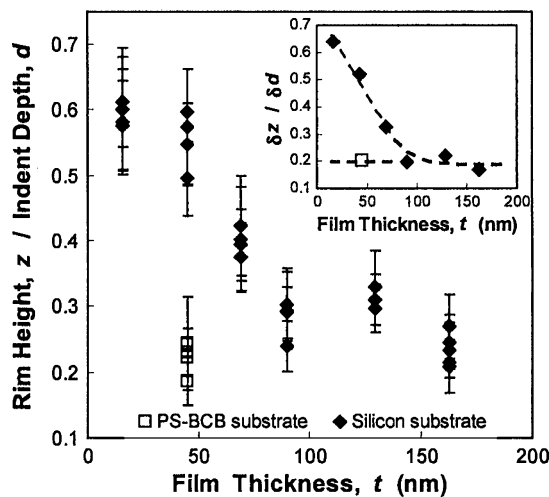


Figure 7. Film thickness effect on the ratio of rim height to indentation depth. (inset) Averaged film thickness effect on the rim height expressed as the slope ratio of  $z(F_N)/d(F_N)$  determined from figure 5. The 45 nm PS film supported on the PS-BCB buffer layer exhibits bulk values.

figure 5. For film thicknesses exceeding  $\sim 100 \text{ nm}$ , the  $z/d$  ratio displays a constant value of approximately 0.2, and reflects the bulk material response. For film thicknesses below 100 nm, the rim height increases with decreasing film thickness. This behavior was found dependent on the substrate material; the 45-nm film on the 230 nm PS-PCB clearly did not display the enhanced rim formation apparent in the 45 nm film supported directly on silicon. This indicates that the rim enhancement phenomenon is related to the distance from the rigid silicon substrate, not the film thickness itself.

Substrate effects during quasi-static indentations, such as enhanced rim heights, are well known for indentation depths exceeding 10–30% of the film thickness [4–7]. However, this high strain rate study clearly reveals that substrate effects are noticeable for residual indentation depths significantly less than 10% of the film thickness. This is not unexpected, as we have established above, that the relatively large plastic deformations are due to high strain rate and inertial effects. In this light, substrate constraints may be more appropriately addressed by considering the depth to which plastic deformation has penetrated into the sample.

Constrained plastic flow can be seen by normalizing the plastic zone radius,  $r_p$ , by the contact radius,  $a_c$  [7]. Our data are plotted under this formalism as a function of the film thickness normalized contact radius,  $a_c/t$ , in figure 8. Recall that we have assumed the plastic radius is equivalent to half of the rim diameter, and  $a_c$  is defined as  $(z + d)/\tan\beta_{\text{TIP}}$ . A collapse of the data onto a single curve is apparent, as noted by [7]. However, we find that the plot is divided into two regimes at  $r_p = t$ , indicated by the solid line in figure 8: (i) for  $r_p < t$ , the plasticity increases with decreasing  $a_c/t$ , (shallower indents); (ii) For  $r_p > t$ ; the plastic radius exceeds the contact radius by a constant multiple of about 25,

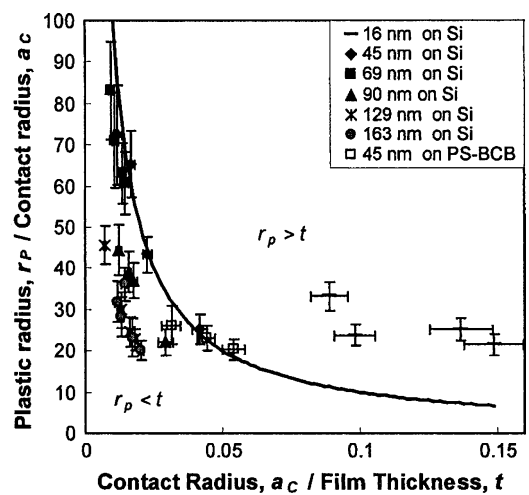


Figure 8. Evolution of the normalized plastic zone radius for increasing indentation depths, expressed in terms of the contact radius with respect to the film thickness. The solid line represents the boundary  $r_p = t$ .

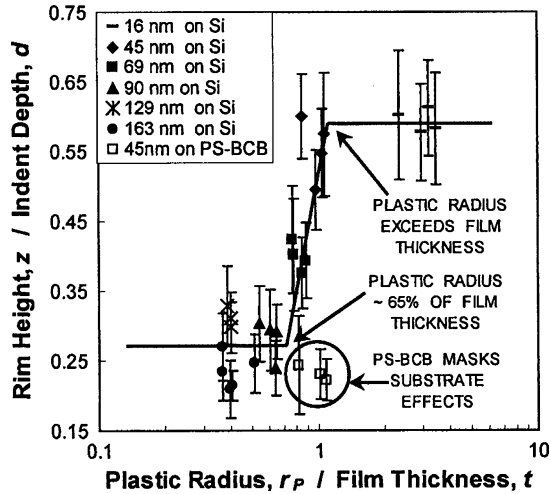


Figure 9. Evolution of the rim height for increasing plastic radius. Strain shielding and higher rims are observed on the silicon supported PS films once the plastic radius reaches 65% of the film thickness. No strain shielding is observed for PS films supported on crosslinked PS-BCB substrates, even when the plastic radius exceeds the film thickness.

indicating that additional plastic deformation is confined at the rigid substrate. Contrary to quasi-static indentation (with an indenter aspect ratio close to one), this transition occurs for a contact radius equal to approximately 4% of the film thickness.

The ratio of the rim height to the indentation depth,  $z/d$ , is revisited in figure 9 as a function of the plastic radius normalized by the film thickness. A sudden increase in the rim height is found when the plastic radius exceeds  $\sim 65\%$  of the film thickness. The rim enhancement occurs because the elastic strain preceding the plastic front is shielded by the rigid substrate, which promotes *upward* deformation. The  $z/d$  ratio levels off once the plastic deformation zone comes into direct contact with the rigid substrate, i.e.  $r_p/t = 1$ . The origin of the plateau for  $r_p/t > 1$  is not entirely clear, but may arise from geometric changes of the plastic domain boundary (spherical to cylindrical) or from an increasing hydrostatic interaction with the substrate. Again, no strain shielding is evident in the PS-BCB supported 45 nm film, even for plastic zone radii in excess of the film thickness. This suggests that, relative to silicon, the modulus and yield stress of the crosslinked PS-BCB are sufficiently similar to the PS homopolymer to promote a more effective stress distribution across the interface. This can be referred to as a *modulus-matched interface*. In the absence of modulus-matching, shear stresses will concentrate at the interface [21], and potentially compromise film stability.

To this point, the large plastic deformation relative to the indentation size has been attributed to the coupled inertial and strain-rate effects under impact conditions, and the rim diameter appears to be the appropriate parameter to address the extent over which plastic deformation has propagated from the indentation site.

So far, we have assumed that the films are homogeneous. Now, let us consider the repercussions of a structural anisotropy of the PS in the vicinity of the substrate. This discussion is motivated by multiple studies of thin films, which suggest strain- and diffusion-induced restructuring over a length scale on the order of 100 nm [22–27]. For instance, an anisotropic interfacial boundary layer in PS films of the same material studied here was shown to impact the glass transition temperature,  $T_g$ , near the substrate [22]. Qualitatively, the nature of the interfacial  $T_g$  profiles in [22] suggests a non-monotonic gradient in the thermomechanical properties. That is, along with  $T_g$ , the modulus is expected to increase with increasing distance from the substrate until a maximum, bulk-exceeding value is reached at roughly 60 nm from the interface. Beyond this point, the modulus is expected to decrease asymptotically to the bulk values at roughly 150–200 nm from the substrate. The formation of these rheological gradients has been attributed to shear-induced structuring during the spin casting process and to anisotropic diffusion during annealing [22,23].

In the current study, the existence of structural anisotropy and its implication on the indentation process are found in analyzing the evolution of the contact pressure with regard to the imposed strain,  $\tan\beta$ . The contact pressure under elastic, elastic-plastic, and fully plastic conditions may be correlated in a dimensionless plot of  $p_m/Y$  as a function of  $E \tan\beta/Y$ , where  $p_m$  is the mean contact pressure defined as  $p_m = F_N/\pi a_c^2$  [8]. The angle  $\beta$  is illustrated in figure 4, and for this analysis, represents the residual plastic strain. With a lack, *a priori*, of any spatial relationship of the film modulus and yield stress, the bulk, quasi-static values reported above are initially assumed. The data are plotted under this assumption in figure 10.

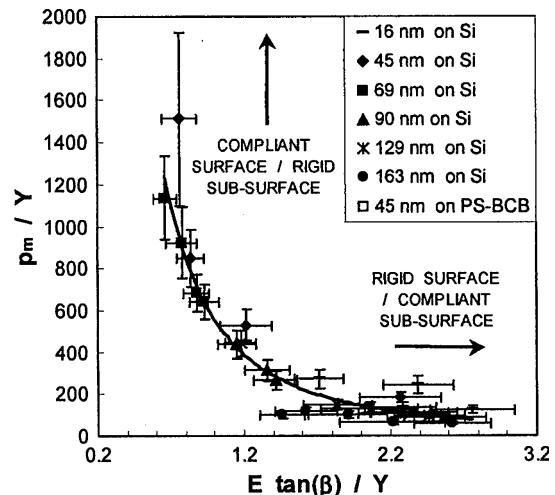


Figure 10. The non-dimensional contact pressure – strain plot reveals a distribution between the two asymptotic behaviors of (i) a compliant surface with a rigid sub-surface and (ii) a rigid surface with a compliant sub-surface.

The qualitative shape of the curve in figure 10 deviates substantially from the isotropic bulk material case, in which the horizontal plateau is attributed to fully plastic deformation with a value of  $p_m/Y \sim 3$  [8]. Recall that the quasi-static, bulk material values for  $E$  and  $Y$  have been used. Strain rate hardening [12–14] is not accounted for; hence, the absolute values in figure 10 are likely inflated and no inference from the absolute values is made. Nevertheless, this systematic error does not preclude a relative analysis regarding film anisotropy.

The collapse of the indentation data into a continuous curve between two asymptotic limits suggests a distribution, or transition, between two mechanical scenarios: (i) a compliant surface with a more rigid sub-surface, represented by the vertical asymptote in figure 10; and (ii) a rigid surface with a more compliant sub-surface, represented by the horizontal asymptote [28].

Conceptually, this may be rationalized as follows: for a compliant surface (lower modulus) with a rigid sub-surface (higher modulus), a finite strain is easily achieved as the surface yields. Additional strain becomes restricted as the more rigid sub-surface is capable of supporting much higher pressures. In the opposite scenario, a critical pressure is required to penetrate the rigid surface. Once the surface has been penetrated, the more compliant sub-surface is incapable of supporting the pressure and succumbs to large strains. Each asymptotic limit has been theoretically predicted for indentations of monotonically graded materials [28]. It is because of the non-monotonic rheological gradient within the thin PS films (see above), that both asymptotes may be observed here in a single experiment.

Interestingly, the vertical asymptote in figure 10 is comprised of indents in films of intermediate thickness, while both thicker and thinner films constitute the horizontal asymptote. The implications of this become apparent when comparing the film thickness dependence of  $p_m/\tan\beta$  to the interfacial  $T_g$  profiles, figure 11. The ratio of  $p_m/\tan\beta$  may be considered an effective modulus, where the pressure is a representation of the applied stress, and  $\tan\beta$  is the resulting strain. Both the relative modulus and relative  $T_g$  are determined by normalizing by the corresponding film thickness dependent values to the bulk values obtained for the thick films ( $t > 150$  nm).

Significant similarities exist between the modulus and  $T_g$  profiles in figure 11. Viewing the glass transition as a mobility barrier, an increase in  $T_g$  offers additional resistance to intermolecular mobility, which intuitively, is accompanied by an increase in the modulus. Hence, the individual thermal and mechanical responses should be expected to coincide. The shape of the thermomechanical profile in figure 11 implies: for films thicker than 150 nm, the material responds like the bulk; for film thicknesses between 60 and 120 nm the surface is more compliant than the immediate sub-surface; and for film thicknesses below  $\sim 60$  nm, the surface is more rigid than the immediate sub-surface. For the last case, one

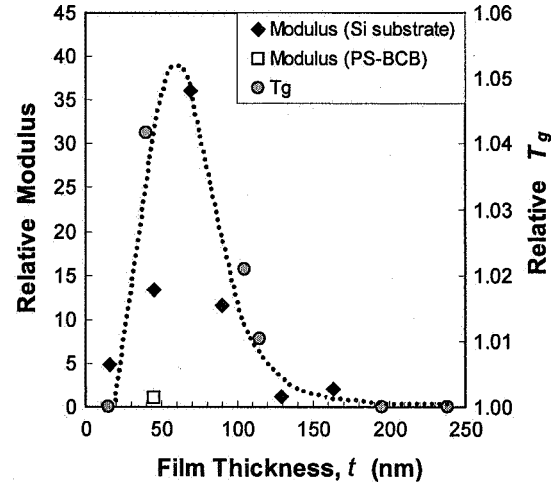


Figure 11. The interfacial thermal and mechanical response profiles for thin PS films are consistent with rheological boundary layer models [22,23], and offer further support of a non-monotonic anisotropic configuration adjacent to the interface. The modulus data were determined from indentations with applied loads ranging between 170–190 nN, and the  $T_g$  data are from [22] qualitatively similar profiles were obtained for all applied loads.

would expect a *negative* rim height or *sink-in* effect [5]; however, strain shielding and confined plasticity at the rigid substrate in the distant sub-surface most likely counterbalance any sink-in tendencies.

The dotted line in figure 11 is drawn so that the film thickness at the peak coincides with the thickness value of the peak in the  $T_g$  profiles determined in [22],  $t \sim 60$  nm. The 45 nm silicon-supported film is somewhat of an anomaly, in that it spans the entire range between both asymptotes in figure 10. While the shallowest indentations in the 45 nm PS-Si film fall on the vertical asymptote, the deepest indentations fall on the horizontal asymptote. This behavior may suggest that the actual peak in the thermomechanical response profile is close to 45 nm from the interface, which is still consistent with the  $T_g$  data obtained on separate films.

#### 4. Conclusions

We have explored how the contact mechanics associated with thermomechanical storage in thin polymer films are compounded by: (i) high strain rates, (ii) the proximity of the underlying substrate, and (iii) material anisotropy near the interface. Strain shielding and confined plasticity at the polymer–substrate interface have led to bulk-deviating mechanical responses, which are manifested through the rim formation process during indentation.

For quasi-static indentations on thin film systems, substrate effects have traditionally been considered with regard to the rule of thumb: they may be avoided for indentation depths less than 10% of the film thickness. Under high strain rate ( $10^3$ – $10^4$  s $^{-1}$ ) impact conditions,

the scenario changes and inertial and high strain-rate effects must be considered. While neither the indentation depths nor the contact radii exceed 10% of the film thicknesses in this study, it is the radial aspect of the piled-up rims that indicates the plastic zone boundary and foretell of substrate constraints.

Strain shielding becomes evident once the plastic radius reaches  $\sim 65\%$  of the film thickness. At this point, the deformation front becomes confined by the underlying rigid substrate. Consequently, enhanced rim heights are observed, and the ratio of the rim height to indentation depth increases from 0.2 in the bulk material to 0.6 when the plastic zone spans the entire film thickness. Interfacial shearing is expected as the plastic boundary is pressed against a rigid interface, possibly activating dewetting instabilities and leading to delamination. In this context, superior film stability would be expected for systems in which the radii of piled-up rims do not exceed the film thickness. However, the mechanical constraints associated with rigid substrates are alleviated with the use of a thick, modulus-matched buffer film (230 nm crosslinked PS-BCB) between the surface film and the substrate.

Rheological anisotropy is apparent in the strain dependence of the contact pressure, and a non-monotonic mechanical gradient within the polymer is corroborated with interfacial glass transition profiles. Under these conditions, the indentation pressures are distributed between two asymptotic limits: (i) a compliant surface with a rigid sub-surface and (ii) a rigid surface with a compliant sub-surface. While enhanced rim formation is expected for the former, and enhanced sink-in for the latter, it appears that, for the given thermomechanical profile, elastic strain shielding and confined plastic deformation at the silicon substrate dominate the anisotropic constraints.

Beyond the immediate implications to the thermomechanical storage process, the work presented here brings a new light to the development of polymer thin film applications. With an understanding of how the interfacial boundary layers are formed [22,23], and knowledge of how they influence rheological behaviors, one could imagine, that the ability to exercise control over the thermomechanical profiles offers a spectrum of possible outcomes: frictional dissipation, wear resistance, and film stability may be engineered for sundry applications. To this end, we foresee a resurgence of design methodologies, moving from the traditional approach of applying special coatings and surface treatments, to one where internal rheological gradients are tailored to achieve the desired performance characteristics.

### Acknowledgments

We gratefully acknowledge the following people for their valuable contributions: Eugene Delenia, Victor Y. Lee, Craig Hawker, Bob Erickson, Victor Chin, and

Chuck Wade from IBM's Almaden Research Center; Urs Duerig, Dorothea Wiesmann, and Michel Despont from IBM's Zurich Research Laboratory; and Arne Biermann from the University of Washington. Funding for this work was provided by IBM.

### References

- [1] G.K. Binnig, G. Gerubini, M. Despont, U.T. Duerig, E. Eleftheriou and P. Vettiger, in: *Springer Handbook of Nanotechnology*, ed. B. Bhushan (Springer-Verlag, Heidelberg, Germany, 2004).
- [2] P. Vettiger, *et al.*, IEEE Trans. Nanotechnol. 1 (2002) 39.
- [3] I. Karapanagiotis, D.F. Evans and W.W. Gerberich, Polymer. 43 (2002) 1343.
- [4] T.Y. Tsui and G.M. Pharr, J. Mater. Res. 14 (1999) 292.
- [5] T.Y. Tsui, J. Vlassak and W.D. Nix, J. Mater. Res. 14 (1999) 2204.
- [6] N.X. Randall, C. Julia-Schmutz and J.M. Soro, Surface and Coatings Tech. 108–109, (1998) 489.
- [7] D.E. Kramer, A.A. Volinsky, N.R. Moody and W.W. Gerberich, J. Mater. Res. 16 (2001) 3150.
- [8] K.L. Johnson, *Contact Mechanics* (Cambridge University Press, Cambridge UK, 1985) 168.
- [9] Schrader D., in: *Mechanical Properties of Polymers*, ed. L.E. Nielsen (Reinhold Publishing Corporation, New York, 1962) V/91.
- [10] C. Creton, J.-L. Halary and L. Monnerie, Polymer. 40 (1998) 199.
- [11] C. Ramond-Angélélis, Analyse mécanique des essais d'indentation sur matériaux élasto-plastiques homogènes ou multi-couches. Application à la caractérisation de la théologie et de la tenue, mécanique des films minces, Ecole Nationale Supérieure des Mines de Paris, 1998.
- [12] G. Dean and B. Read, Poly. Test. 20 (2001) 677.
- [13] H. Zhao, Polymer 39 (1997) 1103.
- [14] H. Eyring, J. Chem. Phys. 4 (1936) 283.
- [15] A. Nayebe, R.E. Abdi, O. Bartier and G. Mauvoisin, Mat. Sci. Eng. A333 (2002) 160.
- [16] C.Y. Chiem, in *Shock Wave High-Strain-Rate-Phenomena in Materials*, ed. M.A. Meyers, L.E. Murr and K.P. Staudhammer (Marcel Dekker, Inc., New York, 1992) 69.
- [17] J.A. Zukas, T. Nicholas, H.F. Swift, L.B. Greszczuk, D.R. Curran, *Impact Dynamics* (John Wiley & Sons, New York, 1982) p. 1–5, 95–150, 279–81.
- [18] L.L. Wang, Chinese J. of Mech. A19 (2003) 177.
- [19] S.M. Walley, J.E. Field, P.H. Pope and N.A. Safford, Philo. Thans. Roy. Soc. London. Series A 328 (1989) 1.
- [20] N. Cristescu, *Dynamic Plasticity* (North-Holland Publishing Co., Amsterdam, 1967), p. 101–179, 335–392.
- [21] A.E. Giannakopoulos, Thin Solid Films. 332 (1998) 172.
- [22] S. Sills, R.M. Overney, W. Chau, V.Y. Lee, R.D. Miller and J. Frommer, Chem. Phys. 120 (2004) 5334.
- [23] S. Sills, J. Frommer, and R.M. Overney, in *Applications of Scanned Probe Microscopy to Polymers*, ed. J.D. Batteas, G.C. Walker, and C. Michaels (American Chemical Society, Washington D.C., 2005) in press.
- [24] R.M. Overney, D.P. Leta, L.J. Fetters, Y. Liu and M.H.J. Rafailovich Sokolov, J. Vac. Sci. Technol. B14 (1996) 1276.
- [25] R.M. Overney, L. Guo, H. Totsuka, M. Rafailovich, J. Sokolov, and S.A. Schwarz. *Interfacially Confined Polymeric Systems Studied by Atomic Force Microscopy* (Material Research Society, 1997).
- [26] R.M. Overney, C. Buenviaje, R. Luginbuehl and F. Dinelli, J. Thermal Anal. Cal. 59 (2000) 205.
- [27] C. Buenviaje, S. Ge, M. Rafailovich, J. Sokolov, J.M. Drake and R.M. Overney, Langmuir 19 (1999) 6446.
- [28] S. Suresh, A.E. Giannakopoulos and J. Alcala, Acta mater. 45 (1997) 1307.